

09,14,15

Structural, Opto-Physical, Photoluminescence, and Optical Limiting Properties of Polyvinyl (Pyrrolidone and Alcohol) Blend Film Doped with Co-Metal

© H. Elhosiny Ali^{1,2,3}, Y. Khairy², M.O. Abdellahi³, M.A. Sayed^{3,4}, H.S.M. Abd-Rabboh^{5,6}, N.S. Awwad⁵, M. Shkir³, M.M. Abdel-Aziz⁷

¹ Research Center for Advanced Materials Science (RCAMS), King Khalid University, Abha 61413, P.O. Box 9004, Saudi Arabia

² Physics Department, Faculty of Science, Zagazig University, 44519 Zagazig, Egypt

³ Advanced Functional Materials & Optoelectronic Laboratory (AFMOL), Department of Physics, Faculty of Science, King Khalid University, P.O. Box 9004, Abha, Saudi Arabia

⁴ Physics Department, Faculty of Science, Al-Azhar University, Assiut 71524, Egypt

⁵ Department of Chemistry, Faculty of Science, King Khalid University, Abha 61413, Saudi Arabia

⁶ Department of Chemistry, Faculty of Science, Ain Shams University, Cairo 11566, Egypt

⁷ Department of Physics, Faculty of Science, Al-Azhar University, Nasr City, Cairo, Egypt

✉ Email: hithamph@gmail.com

Received April 10, 2022

Revised April 15, 2022

Accepted April 15, 2022

The optical properties of polyvinyl (pyrrolidone and alcohol) and PV(P/A) blend polymer have been improved using Co-metal as a filler for optoelectronic and optical shielding applications. The casting technique of solutions was used in order to prepare composite films with different Co-ratios (x : 0–18.5). XRD, FT-IR, SEM, and UV–visible spectrophotometry were operated to study the structure, morphology, and optical features of the flexible plain blend and composite films. The semi-crystalline nature of the films was influenced by the filler ratio of nanoparticles. Homogenous dispersion with some agglomeration of Co-particles has been observed in the host blend matrix. Then again, a successful interaction between the host matrix and particles was ensured by the FT-IR spectroscopic and XRD measurements. The cut-off absorbance edge of composite films is red-shifted from 200 nm (host blend) to 228 nm. The indirect transition optical band gap was confirmed from the Tauc's and optical dielectric loss calculations. Its value goes back from 5.15 eV (plain blend) to 4.43 eV for 18.5 wt% Co-blend composite film. An improvement in the extinction coefficient, optical conductivity, and refractive index of the composite films was achieved compared with the plain blend. The non-linear parameters of the composites were also enhanced. Photoluminescence (PL) emission spectra of PV(P/A) blend films doped with various weight percentages of Co-metal were examined at a wavelength of 750 nm. The optical shielding performance of the prepared composites is recommended for laser cut-off. Furthermore, the ability to tailor the optical properties of blend film makes it more effective for various applications including optical devices, non-linear optoelectronics, and reflective coating.

Keywords: extinction coefficient, PV(P/A) polymer blend, transition band gap, photoluminescence, NL optical parameters, optical shielding.

1. Introduction

Flexible polymers have a wide range of industrial applications due to various sets of properties, such as easy-to-process, anticorrosive, economical, and lightweight [1]. Besides, their mechanical, structural, optical, electrical, and thermal features can be tailored [2]. The mixture of two polymers or more is a way to enhance their efficiency. The resulting mixture is called a blend and the properties are provided in a different set than individual polymers.

Then again, their incorporation with nano-dopants can also change the polymer performance [3–6]. Polyvinyl alcohol (PVA), $(C_2H_4O)_n$, is a semi-crystalline character and due to its appealing physicochemical properties, it can be used as a preferred polymer in a wide range of applications across industries [7–10]. However, the polyvinyl pyrrolidone, $(C_6H_9NO)_n$, is amorphous with a high solubility allowing it to be used in photonics and optics. In addition, PVA and PVP are desired for the encapsulation of different nanomaterials to increase the colloidal stability and fine size

distribution, and decrease agglomeration [11]. In general, PV (A and P) blends have significance to researchers because of their desirable characteristics such as hydrophilicity influence, ecofriendliness, non-toxicity, and biocompatibility as an organic passivating agent on nanomaterials [12,13]. Blend PV (A and P) polymers with inorganic nanodopants, including ceramic ions, semiconductors, metal salts, rare-earth ions, or other additives appropriate in several technological and industrial fields [14]. B.M. Barker [15] examined the effect of cadmium chloride (CdCl_2) on the physical properties of the PV (A and P) blend. According to H. Elhosiny Ali et al. [16], composite films of PV (A and P) incorporated with silver nitrate (AgNO_3) produce new polymeric composites that are beneficial for non-linear optical systems, solar cells, optical limiting devices, and biosensors. S. Choudhary [17] studied the change in the properties of blend films embedded with amorphous silica (SiO_2) nanoparticles.

Cobalt is used for the development of high-performance alloy and the manufacturing of electric vehicles and rechargeable batteries [18]. It can exist in face-centered cubic (FCC) or hexagonal close-packed (HCP) forms or both coordinations [19]. Also, its optical properties have been investigated in different complexes by various authors [20,21]. The coordination number and band position mostly rest on the structure of the composite.

The objective of this paper is to enhance the structural, morphological, and optical properties of polyvinyl (alcohol and pyrrolidone) blend film for the required applications. The morphological and microstructure analysis have been investigated via scanning electron microscopy, FTIR, and X-ray diffraction. The kind of electronic transition through the films has been calculated by different methods. Then again, the possibilities of using the films as optical shielding and linear/non-linear optical materials have been studied.

2. Experimental

2.1. Materials and methods

Amorphous polyvinyl pyrrolidone PVP [$(\text{C}_6\text{H}_9\text{ON})_n$], with molecular weight $M.W.=40,000$ g/mol and semicrystalline polyvinyl alcohol PVA [$(\text{C}_2\text{H}_4\text{O})_n$] with $M.W.=1,15,000$ g/mol were consumed as basic polymeric materials to fabricate polyvinyl (alcohol and pyrrolidone), PV (A and P), polymer blend. The Co-metal powder of 3N purity was provided from Laboratory Reagents & Fine Chemicals (LOBA Chemie), India. Solution casting procedure is employed to make polymeric films of PV(P/A)- x wt% Co by dissolving the components in distilled water.

First, 1000 ml of distilled water with 45 grams of the PVP polymer was stirred using a magnetic stirrer. The same was done for the PVA polymer. After that, both solutions were mixed to form PV(P/A). Various concentrations of Co-metal powder (0, 0.037, 0.37, 3.7, and 18.5 wt%) were ultrasonically dissolved for four minutes into 60 ml of the

blended solution. The mixtures with free bubbles were dried in a warm oven for four days at 40°C , after casting the solutions into 80-mm Petri dishes. The following relationship was used to estimate the weight percentage of Co-metal in the blend matrix:

$$W_{\text{Co}} = \frac{W_{\text{Co}}}{W_{\text{Co}} + W_{\text{b}}} \cdot 100\%. \quad (1)$$

W_{b} and W_{Co} are the weights of polymer blend and cobalt metal. The prepared films were labeled as pure PV(P/A) blend, PV(P/A): 0.037 wt% Co (1Co-blend), PV(P/A): 0.37 wt% Co (2Co-blend), PV(P/A): 3.7 wt% Co (3Co-blend), and PV(P/A): 18.5 wt% Co (4Co-blend).

2.2. Measurements

Shimadzu XRD-6000 Model diffractometer-copper target ($\lambda_{\text{Cu-K}\alpha} = 1.54108 \text{ \AA}$) was used to collect the structure data from the films. This particular XRD operated at a voltage of 40 kV and 25 mA. All samples were scanned at a rate of 0.02/s in a range of $10^\circ < 2\theta < 70^\circ$ to identify all phases. The authors used a Thermo Nicolet 67600 spectrometer operating in the $4000\text{--}500 \text{ cm}^{-1}$ wavelength range to obtain the FT-IR transmission spectra of pure PV(P/A) and composite films. Then again, the scanning electron microscope (SEM) (JSM-6360) has been used to analyze the film's surface morphology.

The UV-visible NIR JASCO V-570 spectrometer worked in the range of 200–1000 nm to measure the transmission and absorption of the films at room temperature. A laser power meter (Lab-Master Ultima-Model, USA) and a 0.1-m focal length lens were used for the optical shielding characterization of the synthetic polymer films. The Fluorolog 3 spectrofluorometer of the HORIBA Jobin Yvon model was used to detect the luminescence of the specimens under an emission wavelength of 470 nm at room temperature.

3. Results and Discussion

3.1. Structural analysis

The structure of the films can be studied with the help of different methods. In the present study, we used X-ray diffraction and FT-IR spectroscopy as presented in Fig. 1, *a* and *b*, respectively. The XRD analysis is an invaluable method for identifying the sample's crystal structure and degree of crystallinity. Fig. 1, *a* shows the diffraction patterns of the pure PV(P/A) blend and composite films. As reported in the previous study, the PVP has a characteristic diffraction peak in the same diffraction range ($18^\circ \leq 2\theta \leq 20^\circ$) of PVA [22,23]. The present patterns indicate that the (101) plane is shown around 19.44° . It is consistent with the intermediate character between crystalline and amorphous phases of the PV(P/A) blend. The semi-crystalline nature of the PV(P/A) blend is due to the strong intermolecular interaction between the

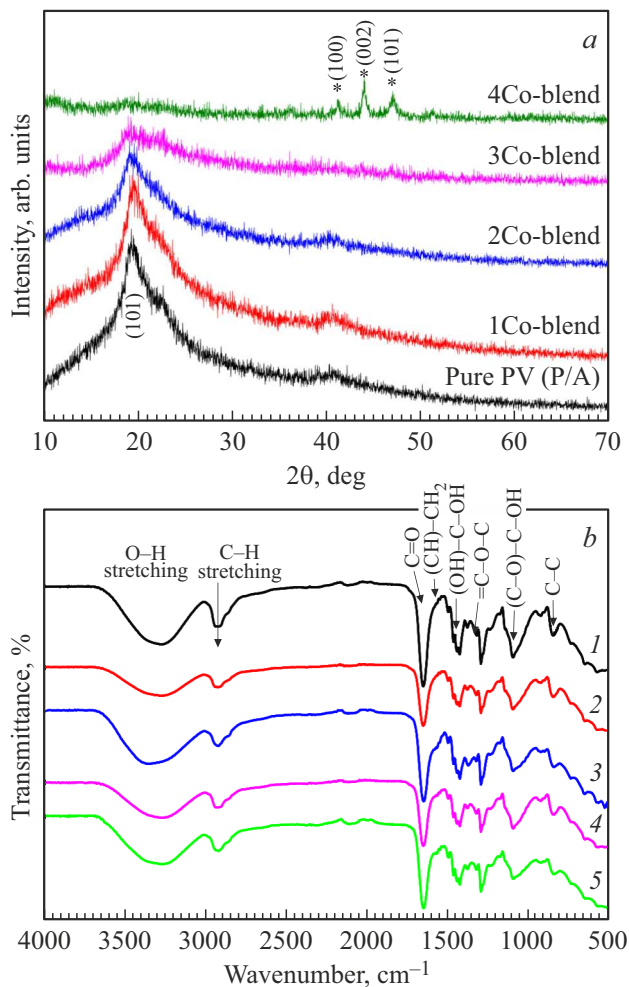


Figure 1. a) XRD patterns and b) FTIR spectra of pure blend and Co-blend composite films.

matrices [24]. Another wide and low-intensity peak was identified at 40.98° . This peak corresponds to the non-crystalline portions in the polymeric matrix [25]. The effect of the Co-metal concentrations on the diffraction pattern of the PV(P/A) blend was demonstrated in the intensity of the peaks. There is a decrease in the intensity of (101). This result is connected to the creation of deformations and defects in the synthesized polymer films due to the greater intermolecular interaction between the matrix and Co-metal. This further led to a variation in the degree of crystallization and a development in amorphous zones [9]. The crystalline (101) peak intensity decreased dramatically as Co-metal was gradually added to the polymeric blend. Furthermore, at low concentrations of Co-metal, no extra peaks of diffraction are observed, whereas the composite film of high concentrations of Co-metal (37 wt%) shows additional peaks. These extra peaks in the pattern 4Co-blend film are denoted by the hexagonal close-packed phase (HCP) of Co-metal. In agreement with previous literature and the database of ICDD-data file 15-0806 [26], the reflections at 41.26 , 44.03 , and 47.07° were assigned to (100), (002),

and (101) HCP metallic phase. In addition, the peaks of crystalline and non-crystalline phases of PV(P/A) mostly disappeared due to the high distribution of Co-metal inside the blended matrix. A similar results have been recognized in many PV(A/P) polymer blend films doped with various materials [5,12,27].

Then again, the intermolecular interactions can be observed by the influence of Co-metal on the functional groups of the blend matrix using FT-IR spectroscopy. This technique was employed to investigate the vibrational spectra of chemical components and functional groups in the materials [28]. FT-IR transmission spectra of pure PV(P/A) and composite films are represented in Fig. 1, b. PV(P/A) blend film exhibits all of the distinct stretching vibrations of the PVP [29] and PVA [19] films with only minor variations in intensities and locations. This verifies that the PVP and PVA are miscible and hydrogen-bonded between their hydroxyl ($-\text{OH}$) and carbonyl ($\text{C}=\text{O}$) groups, i.e., $\text{C}=\text{O} \dots \text{H}-\text{O}$. Stretching $-\text{OH}$ vibrational mode, which seems to be a typical property of the polymer PVA, is seen in the larger band of respectable intensity band centered around 3284 cm^{-1} . C-H asymmetric stretching vibrational mode of either PVP or PVA chains is denoted by a low-intensity band centered around 2924 cm^{-1} . In addition, a strong and intense band at 1647 cm^{-1} is correlated with the C=O stretching vibration of PVP. Other absorption bands are observed at 1487 , 1425 , 1374 , 1319 , 1284 , 1086 , 921 , and 841 cm^{-1} . These peaks correspond to the distinctive vibrations C=N (pyridine ring), CH_2 bending, (CH+OH) bending, CH_2 twisting, C-O stretching or O-H bending, CH_2 rocking, and C-C stretching vibrational modes of PVP [30]. However, as the Co-metal concentration increased in the blend polymer, a modest shift in the bands was observed and the intensities of some separate absorption bands slightly decreased. These performances are similar to the XRD spectra, indicating the adsorption of Co-metal via the functional groups of the blend matrix.

3.2. Microstructural analysis

The phase morphology of the film's surface was examined via scanning electron microscopy (SEM). The influence of Co-metal concentration on the morphological images of the pure PV(P/A) blend is shown in Fig. 2, a-e. The pure blend has a smooth and homogenous surface with tight packing (i.e., a smaller porous structure) indicating the PVP and PVA are well-compatible in the blend (Fig. 2, a) [31]. The pure PV(P/A) surface is well-matched with a previously published polymer blend of the same composition (50/50 wt%) [24,27,32]. In the SEM images of the composite polymer films (Figs. 2, b-e), we can see the dispersion of Co-metal particles (white representations). The addition of doping causes a considerable variation in the surface morphology of pure PV(P/A) film. Initially changing into a hazy shape at low concentration levels (0.037 wt% Co), which floats throughout the entire surface. This demonstrates the homogeneity of distribution at a

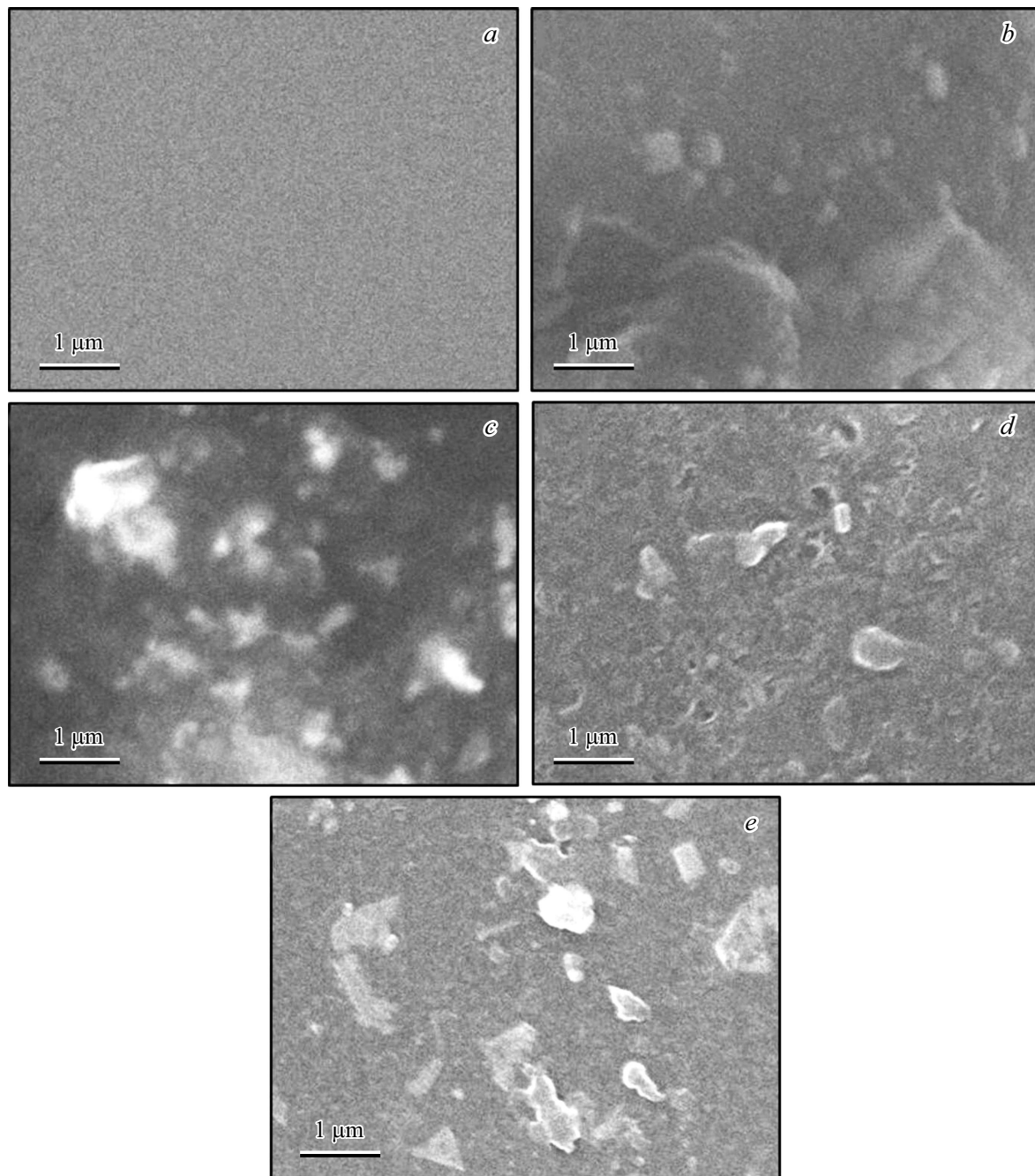


Figure 2. SEM micrographs of the synthesized polymer blend films: *a*) PV(A/P), *b*) 1Co-blend, *c*) 2Co-blend, *d*) 3Co-blend, and *e*) 4Co-blend.

low concentration of Co-metal in the PV(P/A) structure. Then again, the surface morphology changes to rough at a comparatively high concentration (18.5 wt% Co). This reflects the dopant distribution changes depending on the concentration used. As the concentration of dopant increases, the adhesion between the Co-metal and PV(P/A) blend reduces causing the aggregation of the particles (Fig. 2, *c–e*). The morphological studies of the composite films reveal that different sizes, shapes, and distributions of the particles depend on the Co-dopant content. The

4Co-blend film has a distinctive morphology with a greater specific surface area of aggregated Co-particles, which can improve the optical absorption.

3.3. Optical studies

3.3.1. Transmittance and absorbance spectra

The spectral distributions of transmittance $T(\lambda)$ and absorbance $A(\lambda)$ were measured to know more about the opti-

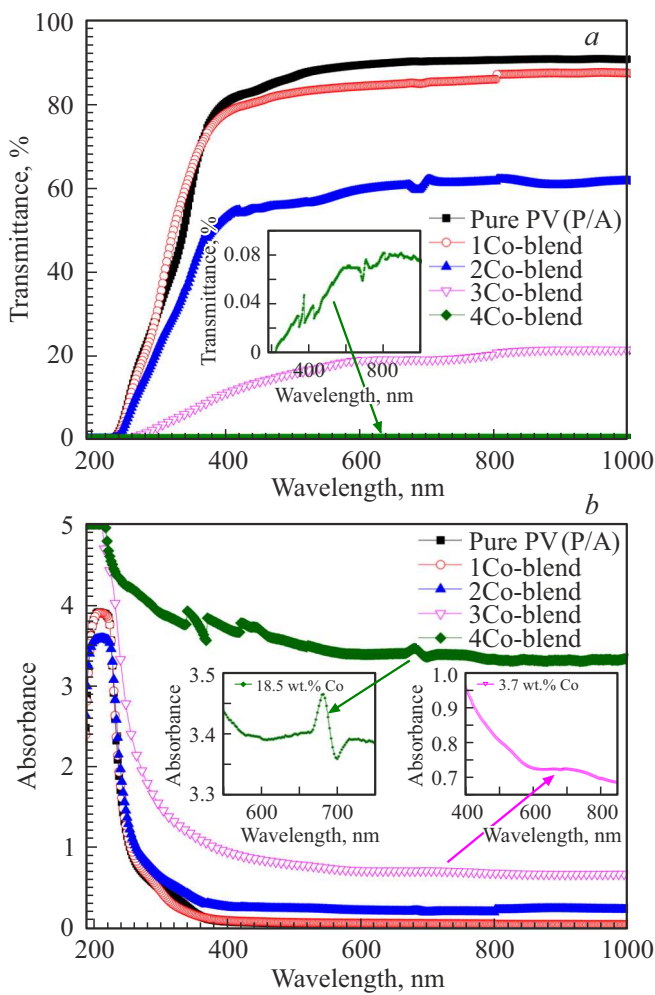


Figure 3. Optical *a*) transmittance and *b*) absorbance spectra.

cal features of the current system. Both spectra are shown in Fig. 3 for the PV(P/A) blend filled with varying quantities of Co-metal in the wavelength region of 200–1000 nm. Pure blend film has a maximum transmission of around 91.5% (Fig. 3, *a*). This subsequently decreased to nearly zero as the amount of Co-metal increased up to 18.5 wt%. The decline in transmittance properties with cobalt concentration can be related to the formation of extra intermolecular bonds within the entire blend matrix. Thus, new defect states were created in the band gap, which acted as light-scattering centers and reduced incident light transmission. The results were validated by SEM micrographs. The particles aggregate with rising doping and hence more incident photons are absorbed or reflected, which limits transmission dramatically [9,19]. Consequently, the films containing a high concentration of cobalt are promising for a multipurpose and attractive flexible material in cut-off laser, UV-block, and optoelectronic applications. This is confirmed by the absorption spectra (Fig. 4, *b*) of the films. A prominent absorption edge can be found at 278 nm for the pure PV(P/A) blend. Then again, the absorbance

is approximately zero in the region beyond 400 nm. The absorbance rises with increasing Co-metal content and the absorption edge progressively shifts towards higher wavelength regions (red shift). This indicates that the optical energy band gap of these materials was reduced. Most organometallic materials have excellent optical absorption and emission properties within wavelengths ranging from

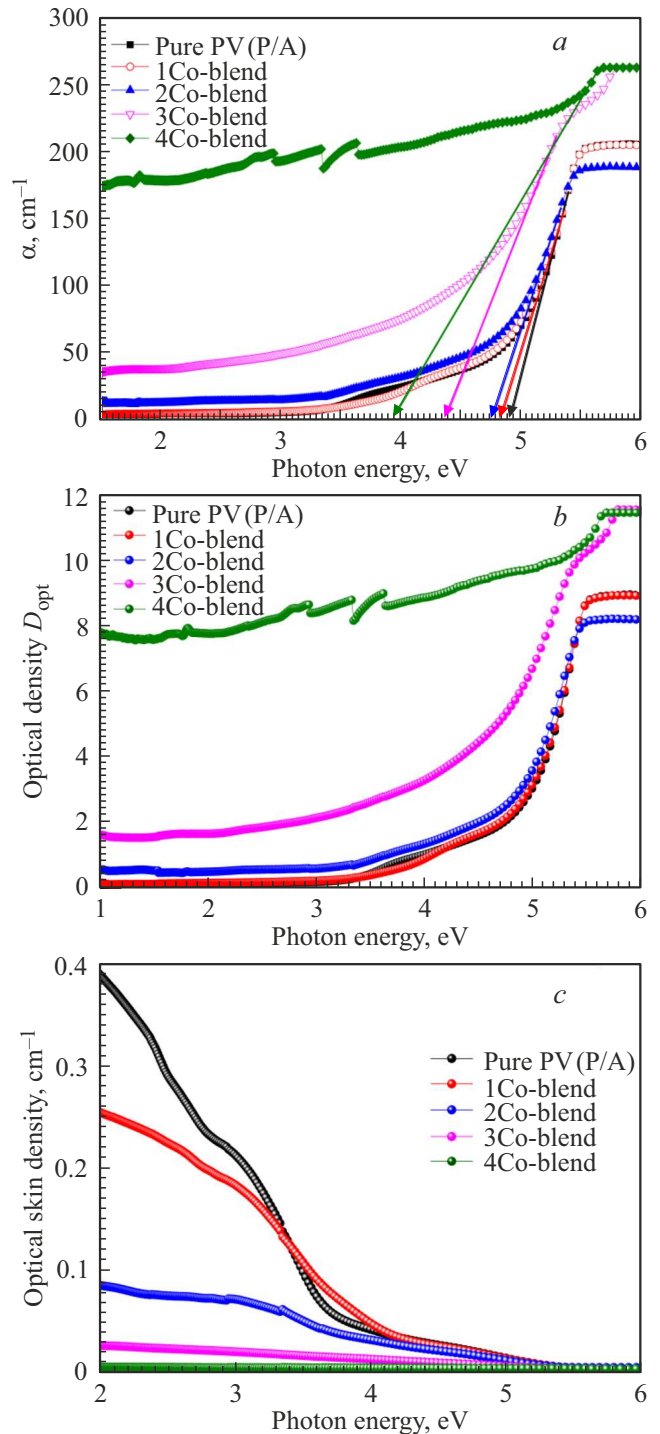


Figure 4. *a*) Coefficient of optical absorption α , *b*) optical density, and *c*) optical skin depth as functions of the photon energy.

600 to 700 nm [32,33]. This can be based on the orbital overlapping and the assistance of ligands. So, electrons can transfer through the structure, which gives rise to absorbance [34]. In the range of 600 to 700 nm, the 3Co-blend film exhibits a broad and weak absorption band, as shown in Fig. 3, *b*. This band begins to improve as the Co-metal content increases to 18.5 wt% (4Co-blend) due to the particle's surface plasmon resonance (SPR) property in the composite polymer films. The SPR is essentially a high-density free electron (plasmon) oscillation of an optoelectronic material that occurs when it is exposed to light energy. Consequently, the polymer materials are suitable for use as switchable photosensors for an optoelectronic device because their increased surface area to volume ratio accounts with the increase in the SPR peak intensity [35–37].

3.3.2. Absorption coefficient, optical density, and penetration depth

The analysis of the absorption coefficient is essential to investigate the changes in the band structure of polymeric material [38–41]. In addition, it gives valuable information about the energy of the optical prohibited gap. The Beer–Lambert–Bouguer equation is normally used to compute the absorption coefficient [42]:

$$\alpha = \frac{2.303 \cdot A(\lambda)}{d} \quad (2)$$

$A(\lambda)$ and d (measured in cm) are the optical absorbance and the thickness of the polymer films. The correlation between optical absorption coefficient α and incident photon energy $h\nu$ is shown in Fig. 4, *a*. It is possible to determine the absorption edge's energy by extending the absorption graph's line to intersect the x -axis at the location of zero absorption coefficients. Table 1 displays the estimated absorption edge energy values for the films under investigation.

The absorption edge of pure PV(P/A) is 4.86 eV. This value shifted to the lower energy of 3.85 eV for 4Co-blend. The decrease in absorption edge is caused by the production of localized states in the band gap associated with the generation of defects in the films [42].

However, the tendency of a material to absorb electromagnetic waves can be described by the optical density.

This metric is significant to describe the effect of the composition concentration, structure, and the application suitability of the polymer films. The difference between the coefficient of absorbance α and optical density D_{opt} is small. D_{opt} is proportional to both α and the film thickness d . It is computed using the formula [40]:

$$D_{\text{opt}} = \alpha d = 2.303 A(\lambda) \quad (3)$$

The variation of D_{opt} with the photon energy is shown in Fig. 4, *b*. It demonstrates that raising the Co-metal concentration results in an increase in optical density.

On the other hand, the penetration depth is a critical optical factor for light absorption in thin films. It is essential for the implementation of polymer films in optoelectronic applications. The penetration depth δ is inversely proportional to the absorption coefficient α as following the formula [42],

$$\delta = 1/\alpha \quad (4)$$

Fig. 4, *c* presents the relation between penetration depth and incident photon energy. The result indicates that as the optical transmission reduces with increasing Co-metal concentrations, the penetration depth decreased. This means that the skin thickness of the synthesized polymer films declines exponentially and approaches practically zero at 5.44 eV with increasing the incident light energy. The energy of the zero penetration depth is known as the cut-off energy, $E_{\text{cut-off}}$, and the associated wavelength (228 nm) is called the cut-off wavelength, $\lambda_{\text{cut-off}}$. However, the influence of incident photons on the skin thickness is nearly negligible throughout the entire range of investigated energy for 4Co-blend film because of the strong absorption properties.

3.3.3. Optical band-gap and Urbach tail energies

The optical and electrical characteristics are experimentally characterized as a function of the band gap. A vital method for estimating the value and nature of the optical band-gap energy of each material is using the absorption spectra, which correlate with the electronic transition from the valence band to the conduction band [9,37]. The electronic transitions that occur in the material are typically reliant on the intrinsic properties and the energy of the incident photons. The optical absorption intensity is proportional to the energy difference between the incident

Table 1. Optical absorption edge, Urbach energy, and direct and indirect band gap parameters of all present films.

Films	E_e , eV	E_U , eV	$E_{\text{gd}}^{\text{opt}}$, eV	$E_{\text{gt}}^{\text{opt}}$, eV	$E_{\text{opt}}^{\text{dielectric}}$, eV
Pure PV(P/A) blend	4.858	0.992	4.567	5.157	5.307
1Co-blend	4.815	1.030	4.447	5.127	5.296
2Co-blend	4.694	1.642	4.324	5.080	5.201
3Co-blend	4.264	1.969	3.312	4.662	4.896
4Co-blend	3.853	2.187	2.670	4.433	4.394
PV(A/P): 0–5 wt% SiO ₂ [17]	–	1.93–1.35	5.19–4.98	5.05–4.92	–
PV(A/P): 0–3.7 wt% AgNO ₃ [16]	5.09–3.35	0.951–2.459	5.582–4.157	4.671–2.744	–

beam ($h\nu$) and the forbidden/band gap energy (E_{opt}). In the strongest absorption section, the relationship between the absorption coefficient α and incidence radiation energy $h\nu$ can be understood in the context of Tauc's formula

$$(\alpha h\nu)^r = \beta(h\nu - E_{\text{opt}}). \quad (5)$$

It is worth noting that β is the band tailing parameter, which is an energy-independent constant, and r is the transition-mode power factor, whose magnitude depends on the crystalline or non-crystalline nature of the material. The relationship between $(\alpha h\nu)^r$ on the y -axis and $h\nu$ on the x -axis is presented in Fig. 5. There is a distinct linear domain in the resulting graphs that correspond to the material's absorption onset. The value of the forbidden gap of the examined polymer films was determined by extrapolating the linear segment until it intersects with the $h\nu$ -axis. r is equal to 2 for allowed direct transitions and $1/2$ for allowed indirect transitions. The direct and indirect permitted optical transitions of the as-prepared polymer films are shown in Fig. 5, *a* and *b*. The result of the permitted direct and indirect optical band-gap transitions is seen in Table 1. Their values for the pristine and composite [(PV(P/A) — x wt% Co)] films were decreased from 4.57 to 2.67 eV and 5.16 to 4.43 eV, respectively. By correlating the structure and microstructure analysis with the optical properties, we can conclude that the decrease in blend band gap is related to the change in the matrix disorder. In addition, it is associated with the complex electron transport as a result of trapped levels within the band gap between LUMO and HOMO of the blend matrix resulting in a reduction in electron transfer energy [16]. This demonstrates the miscibility of cobalt-metal particles with the PV(P/A) matrix.

The material's band tail width is described by the exponential interpretation of the absorption coefficient graph. The band tail is generated due to defect states caused by doping. The density of localized defect states varies exponentially with the incident photon energy [43]. The Urbach energy characterizes the width of the band's tail as a result of defect states, which are associated with disordered or non-crystalline materials. The following relationship was proposed by Urbach as an empirical model to estimate Urbach tail energy [44]:

$$\alpha = \beta_0 \exp\left(\frac{E}{E_U}\right). \quad (6)$$

β_0 and E_U are constant and Urbach tail energy. The reciprocals of the straight-line slopes of Fig. 5, *c* are the Urbach energy of each film. The values are shown in Table 1. The E_U increased from 0.99 eV to 9.79 eV with an increase in Co-metal content, indicating an increase of traps in the forbidden gap [45]. These results are consistent with the optical band gap attitude. The reduction in the prohibited gap is caused by the formation of localized states. Thus, the increase of the tail width results in a decrease in the band-gap energy. Several polymer films exhibit these inversely proportional attitudes between E_{opt} and E_U [46].

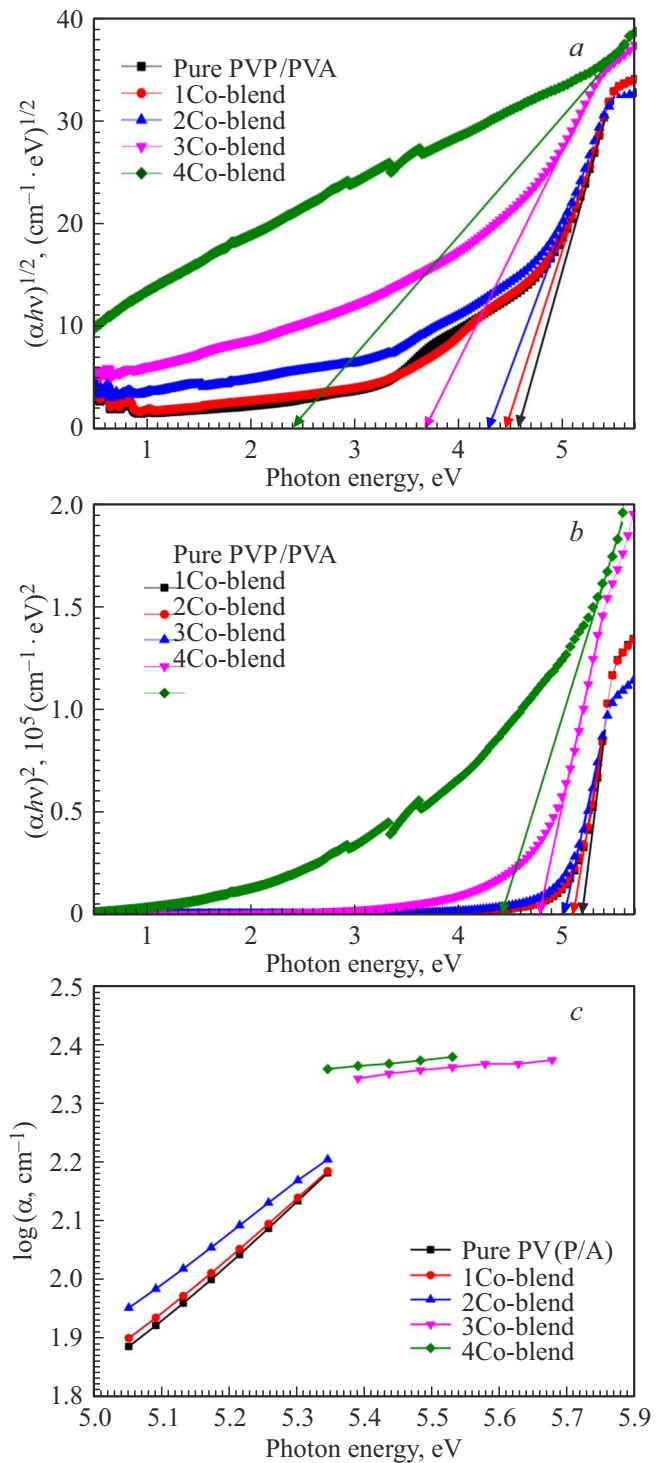


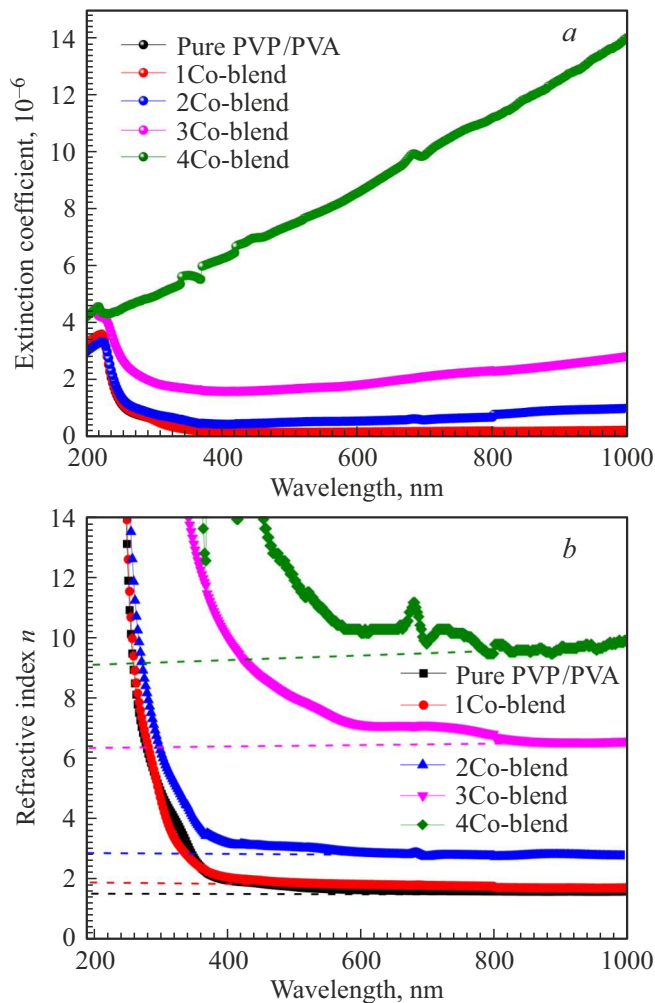
Figure 5. Tauc's relation for *a*) indirect and *b*) direct transitions, and *c*) $\ln \alpha$ versus incident photon energy $h\nu$ for composite films with different Co-metal concentration.

3.3.4. Optical extinction coefficient, refractive index, dielectric loss, and conductivity

The optical extinction coefficient k is one of the significant parameters in optical absorption devices that gives valuable

Table 2. Linear and non-linear refractive index and susceptibility

Films	n	$\chi^{(1)}$, e.s.u.	$\chi^{(3)} \cdot 10^{-10}$, e.s.u.	$n_2 \cdot 10^{-10}$
Pure PV(P/A) blend	1.473	0.093	1.28E-4	3.266E-3
1Co-blend	1.741	0.162	1.16E-3	2.512E-2
2Co-blend	2.644	0.477	8.78E-2	1.252
3Co-blend	6.201	2.980	134.13	815.45
4Co-blend	7.217	4.065	464.29	242.53

**Figure 6.** a) Extinction coefficient and b) refractive index as functions of wavelength.

insight into the light beam transferred across a material. The k value represents the percentage of photons absorbed or dispersed per unit length through the penetrating medium. It is an imaginary part of the complex refractive index, $\bar{n} = n - ik$, and calculated using the formula, $k = \alpha\lambda/4\pi$ [47]. Fig. 6, *a* shows the relation between the absorption index k and the photon wavelength λ . It is noticed that k -values are found to decrease significantly as the wavelength increases from 200 to about 420 nm in the UV region and then becomes approximately constant

in the visible range for pure and composite films with low Co-metal concentrations. These low values are a result of the high optical transmission of the films in that region. However, by raising the Co-content, the k -values increased dramatically. This result is because the optical absorption properties of composite films are enhanced. Mott and Davis found a consistent tendency in a variety of materials including low-crystalline and non-crystalline materials [48].

Another factor critical in optical applications is the index of refraction of the materials. It is connected to the electronic polarization and local fields within optical materials [49,50]. The refractive index n can be calculated using the following simplified relation as a function of reflection R [51]:

$$n = \frac{1 + \sqrt{R}}{1 - \sqrt{R}}. \quad (7)$$

Refractive index versus wavelength is shown in Fig. 6, *b* for all synthesized polymer samples. The composite films display a dispersion performance as a function of wavelengths. According to our findings, the refractive index of pure blends increased from 1.47 to 9.06 by incorporating Co-metal (Table 2).

The metal particles lead to an increment in the number of free carriers and the reflection of the polymer films causing an increase in the refractive index value [52]. Then again, it is inversely proportional to the optical energy gap. These characteristics appear to be beneficial due to their application in the development of high-performance optical polymeric materials.

The refractive index and extinction coefficient parameters are essential for calculating the dielectric constants of the material. Several optoelectronic devices depend on the optical dielectric properties including printed circuit boards. The dielectric constant ϵ^* is expressed as a complex quantity of the real and imaginary parts denoted by ϵ_r and ϵ_i :

$$\epsilon^* = \epsilon_r + i\epsilon_i. \quad (8)$$

The deceleration of a light wave as it travels through a film material is characterized by ϵ_r for any damped oscillator. Consequently, it takes into consideration the light propagation and stored energy in the substance. On the other hand, ϵ_i refers to the amount of light that is absorbed or dissipated within the material. It is proportional to the dispersion and loss of energy inside the material caused by the movement of the electromagnetic wave. Also, it

is named a damping factor. The real (ϵ_r) and imaginary (ϵ_i) components of the dielectric constant are given by the formulae [33]:

$$\epsilon_r = n^2 - k^2, \quad (9)$$

$$\epsilon_i = 2nk. \quad (10)$$

Fig. 7, *a* illustrates the variation of ϵ_r as a function of the incident photon's wavelength. The ϵ_r component has the same behavior as the refractive index and the extinction coefficient. Values of ϵ_r are significantly increased with doping content. Its change with wavelength indicates the existence of significant interactions between the electromagnetic waves and free electrons in the samples. The increment of ϵ_r signify that the dispersion increases with the concentration of Co-metal. Thus, Co-metal is essential for the propagation of light at a slower rate. However, it is observed that with rising cobalt particles in the polymer matrix, ϵ_i increase (Fig. 7, *b*). Its smaller value reflects that less energy is lost. Raising the imaginary component ϵ_i with Co-content indicates an increase in the energy loss by the synthesized polymer films.

Moreover, the relation between the optical dielectric loss ϵ_i and the incident photon energy can be used to estimate the band gap of the samples and specify the kind of electronic transition. The optical dielectric loss can be also represented according to the quantum mechanics as follows [53]:

$$\epsilon_i = \frac{4\pi^2 e^2}{m^2 \omega^2 V} \sum_{v,c,k} |\langle \Psi_{c,k} | p^a | \Psi_{v,k} \rangle \delta(E_{c,k} - E_{v,k} - \hbar\omega), \quad (11)$$

where m , V , ω , $\Psi_{c,k}$, and $\Psi_{v,k}$ are the mass of the electron, the unit cell volume, photon angular frequency, and the crystal wave functions of (occupied and unoccupied) electronic states, respectively [54], whereas the summation is done over the conduction and valence bands. This relation specifies that the optical dielectric loss is connected with the structure of the band ($E_{c,k} - E_{v,k}$). The band edges of the non-crystalline materials are influenced by different metallic complex and ligand orbitals. Thus, it is difficult to determine whether the electronic transition is direct or indirect type [55]. Fig. 7, *b* displays the optical dielectric loss for pure PV(P/A) blend and composite films as a function of the photon energy. The intersection of the extrapolation of the linear portion of the optical dielectric loss with the energy axis is the optical band gap. Their values show that the electronic transition is indirect, after comparing with Tauc's result. The optical band gap arising from the dielectric optical loss spectra are summarized in Table 1.

The optical conductivity σ_{opt} is generated as a result of the excitation of charge carriers as a result of the changes in the electric field of the incident photons. It is determined as a function of refractive index n and absorption coefficient [16]:

$$\sigma_{opt} = \frac{n\alpha c}{4\pi}, \quad (12)$$

where c is the speed of light.

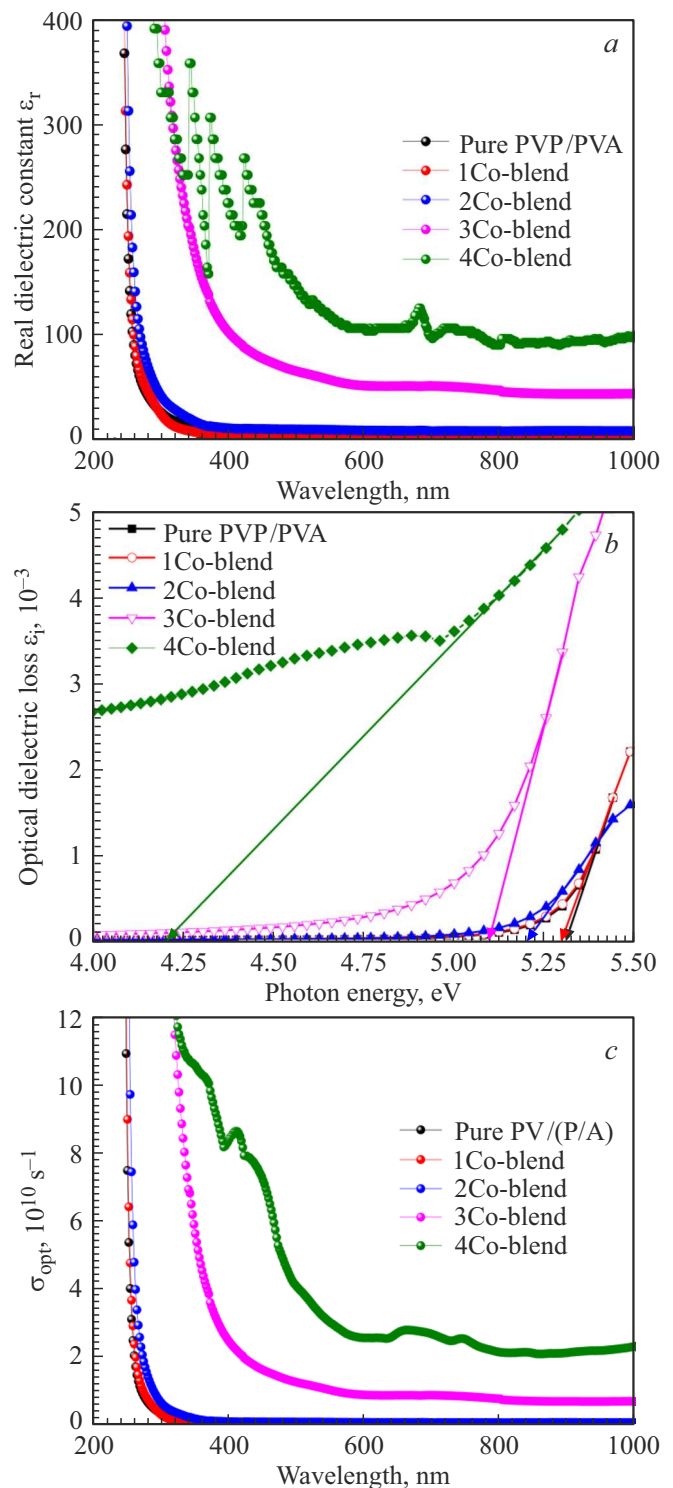


Figure 7. Optical *a*) dielectric constant, *b*) loss, and *c*) conductivity of the pure and composite films.

Fig. 7, *c* depicts the wavelength dependence of optical conductivity for all prepared films. The optical conductivity is greatest at small wavelengths and nearly steady at higher wavelengths. In addition, as the percentage of the Co-metal is increased in the polymer matrix, the optical conductivity

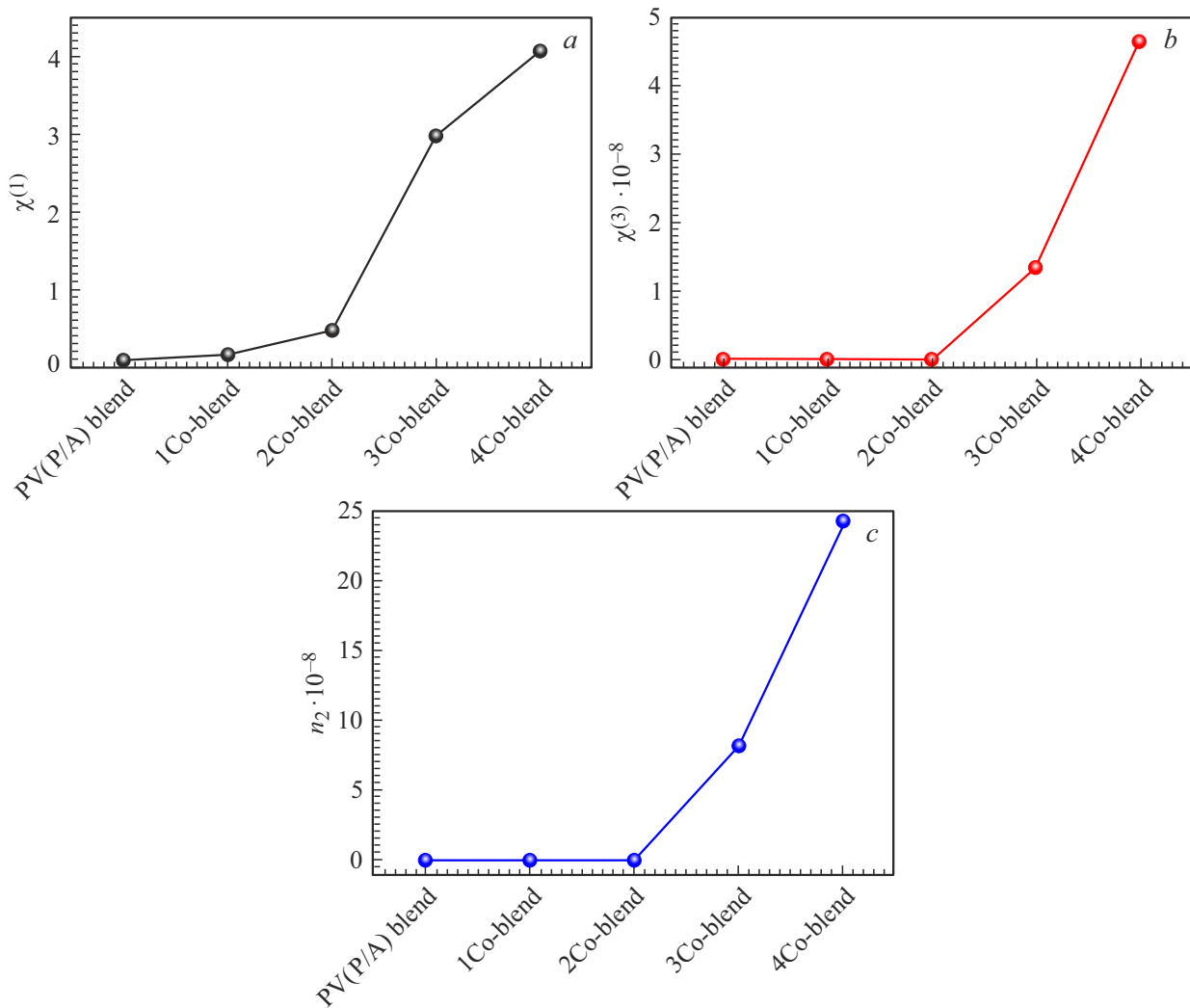


Figure 8. a) Linear susceptibility, b) NL susceptibility, and c) NL refractive index of the pure and composite films.

of the material was improved. This is a result of new defect states being created within the band, which increases the probability of electron transitions from the valence to conduction bands.

3.3.5. Non-linear optical parameters

For non-linear (NL) optical applications, the light effect on the samples was studied. The NL performance was observed as the interaction of the high-intensity light (such as a laser) with the materials. The high-order optical susceptibility gives information about the sample withstanding a high pulse through higher-order effects. The induced polarization, P , is NL proportional to the electric field, E , of the incident light. Thus, NL parameters including refractive index (n_2), 2nd order ($\chi^{(2)}$), and 3rd order ($\chi^{(3)}$) susceptibilities were studied for the present films. The third-order NL optical susceptibility was calculated using the equation [56]:

$$\chi^{(3)} = a(\chi^{(1)})^2, \quad (13)$$

where a is constant and equals to $1.7 \cdot 10^{-10}$ esu and $\chi^{(1)}$ is the linear susceptibility, which is expressed by the following formula

$$\chi^{(1)} = \frac{n^2 - 1}{4\pi}. \quad (14)$$

However, the NL refractive index n_2 can be calculated using the relation

$$n_2 = \frac{12\pi\chi^{(3)}}{n}. \quad (15)$$

The results of NL parameters are tabulated in Table 2. It is noticed that as cobalt concentrations rise, the polarization of the polymer film was enhanced. Thus, the NL parameters were improved as seen in Fig. 8. Therefore, the present polymer films can be used in NL optoelectronic devices.

3.3.6. Limiting absorption analysis

Optical limiter (OL) devices with a significant transmission for low incident photons intensity are considered a novel application [9]. Whatever the intensity of the incident

light beam, the impact of the optical limiters maintains the amount of energy, irradiance, power, and fluency transmitted by an optical device below the incident light's maximum value. One of the main popular uses of this phenomenon is to protect sensitive sensing devices from laser damage [57]. Two different types of laser sources (He–Ne and green laser sources) with wavelengths of 632.8 and 533 nm were used to characterize the OL of the synthesized polymer films. As illustrated in Fig. 9, *a*, the output power levels of the two laser sources have become high for pure blend and 1Co-blend films. Consequently, increasing the concentration of Co-metal in the blend matrix to 18.5 wt% reduces the output power dramatically, resulting in more laser beam blocking. This means that OL features depend heavily on doping proportions. Both sources have different output power ratings because the polymer film reacts differently to incident photons. When Co-metal concentration is increased (18.5 wt%), UV-visible light is completely absorbed, as evidenced by the transmittance and absorbance values for the produced polymer films (Fig. 4). Since the films contain

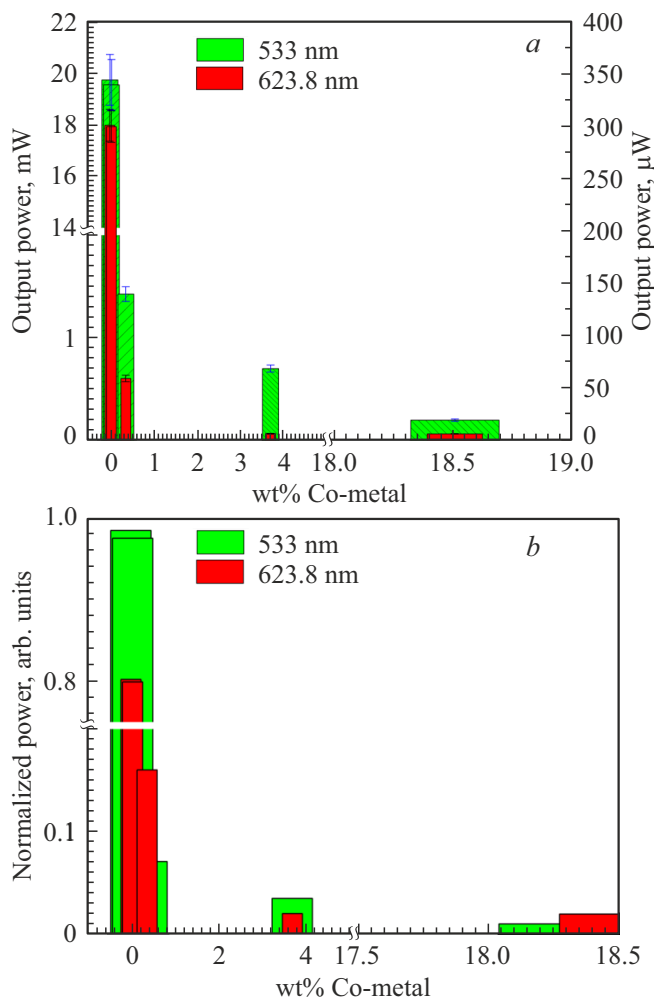


Figure 9. The plot of *a*) output and *b*) normalized power vs concentration of Co-metal for two wavelengths of 632.8 and 533 nm.

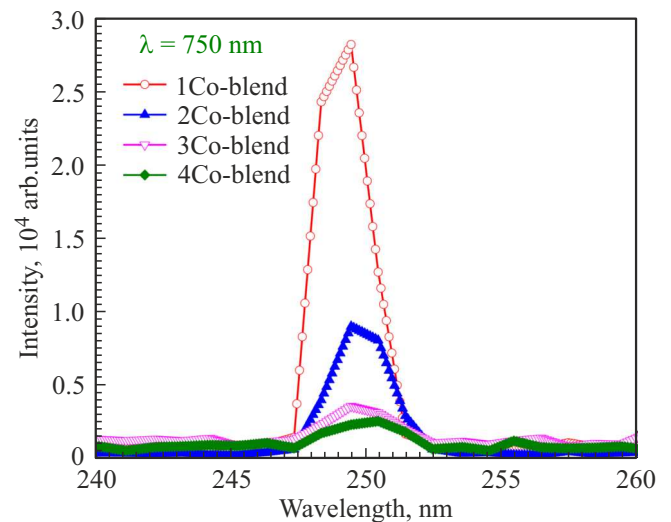


Figure 10. Photoluminescence spectra of pure and Co-doped PV(P/A).

a higher proportion of Co-metal powder, the matrix of the polymer PV(P/A) blend would have an extra molecule per unit volume. Those participate in optical interactions during non-linear absorption mechanisms [9]. Therefore, the OL properties of the studied polymer films are associated with the sample's ability to absorb and scatter light. Fig. 9, *b* shows that the 4Co-blend polymer sample had the minimum normalized power value, which is close to zero. Hence, the new polymer film can be utilized as a cut-off for laser because the light's strength has been reduced and blocked.

3.4. Photoluminescence spectra analysis

The PL emission spectra of PV(P/A) blend films doped with various weight percentages of Co-metal ($x = 0.037, 0.37, 3.7, \text{ and } 18.5 \text{ wt\%}$) and exposed to laser red radiation at a wavelength of 750 nm are shown in Fig. 10. As seen in the figure, there is only one strong PL peak at approximately 250 nm for a blend containing a low dopant Co-metal concentration (1Co-blend). This behavior indicates the formation of defects and imperfections in the polymer blend matrix. As the concentration of Co-filler was raised, the intensity of the PL peak for the doped blend was reduced significantly and became broader. This may occur as a result of clustering of Co particles at higher doping concentrations, which reduces the polymer's surface area [5]. A change in the number of free electrons in material under the influence of light and changes in the number of non-radiative defects on the materials' surfaces may be responsible for either an increase or decrease in the PL peak intensity.

4. Conclusions

Herein, composite films of polyvinyl (pyrrolidone and alcohol), PV(P and A), with 1 : 1 ratio and different

percentages of Co-metal were simply prepared via the casting solution method. The XRD and transmission FT-IR spectra ensure the successful incorporation of PVP, PVA, and Co-particles. Compared with the plain blend polymer, clear changes in the diffraction and transmission IR intensity were observed in the composite films. The surface roughness of the composite films was boosted by the argument of filler ratio. This leads to an enhancement in the absorption performance of composites. Then again, the linear optical parameters of the plain bend matrix were tuned by Co-content. The UV-visible behavior demonstrates the ability to tune the optical properties of blend polymer via Co-particles as a filler. The cut-off absorbance edge of the plain film was shifted from 200 to 280 nm. In addition, the Urbach energy of the prepared composite films is going back from 0.99 to 9.78, which affects the transition band gap value. It is also observed that the linear optical susceptibility $\chi^{(1)}$, extinction coefficient k , dielectric constants ϵ_r and ϵ_i , conductivity σ_{opt} , and refractive index n of the composite films are improved compared with those of the host blend. Along with that the non-linear parameters $\chi^{(3)}$ and n_2 were raised to $464.29 \cdot 10^{-10}$ e.s.u and $242.5 \cdot 10^{-10}$. Thus, the prepared Co-particles filled composite films are effectively utilized in multi-application optical devices.

Funding

The authors extend their appreciation to the Deanship of Scientific Research at King Khalid University for funding this work through the research groups program under grant number R.G.P.1/239/41.

Conflict of Interest

The authors declare that they have no known competing financial interests or personal relationships that could have appeared to influence the work reported in this paper.

References

- [1] A.Y. Yassin. *J. Mater. Sci.: Mater Electron.* **31**, 21, 19447 (2020). <https://doi.org/10.1007/s10854-020-04478-1>
- [2] N.M. Deghiedy, S.M. El-Sayed. *Opt. Mater.* **100**, 109667 (2020). <https://doi.org/10.1016/j.optmat.2020.109667>
- [3] M.T. Ramesan, M. Varghese, P. Jayakrishnan, P. Periyat. *Adv. Polymer Techol.* **37**, 1, 137 (2018). <https://doi.org/10.1002/adv.21650>
- [4] X. Wang, C.G. Bazuin, and C. Pellerin. *Polymer* **57**, 62 (2015). <https://doi.org/10.1016/j.polymer.2014.12.006>
- [5] K. Rajesh, V. Crasta, N.B. Rithin Kumar, G. Shetty, and P.D. Rekha. *J. Polymer Res.* **26**, 4, 99 (2019). <https://doi.org/10.1007/s10965-019-1762-0>
- [6] N. Abu Bakar, C.Y. Chee, L.C. Abdullah, C.T. Ratnam and N.A. Ibrahim. *Mater. Design (1980–2015)* **65**, 204 (2015). <https://doi.org/10.1016/j.matdes.2014.09.027>
- [7] H. Elhosiny Ali, and Y. Khairy. *Physica B* **570**, 10, 41 (2019). <https://doi.org/10.1016/j.physb.2019.05.050>
- [8] H. Elhosiny Ali, H. Algarni, and Y. Khairy. *Opt. Mater.* **108**, 110212 (2020). <https://doi.org/10.1016/j.optmat.2020.110212>
- [9] H. Elhosiny Ali, and Y. Khairy. *Opt. Laser Technol.* **136**, 106736 (2021). <https://doi.org/10.1016/j.optlastec.2020.106736>
- [10] M.M. Abdel-Aziz, H. Algarni, A.M. Alshehri, I.S. Yahia and H. Elhosiny Ali. *Mater. Res. Express* **6**, 12, 125321 (2019). <http://dx.doi.org/10.1088/2053-1591/ab56d8>
- [11] S.O. Aisida, I. Ahmad, and F.I. Ezema. *Physica B* **579**, 2, 411907 (2020). <https://doi.org/10.1016/j.physb.2019.411907>
- [12] A. Badawi. *Appl. Phys. A* **126**, 5, 335 (2020). <https://doi.org/10.1007/s00339-020-03514-5>
- [13] S. Mallakpour, and S. Mansourzadeh. *Ultrasonics Sonochem.* **43**, 91 (2018). <https://doi.org/10.1016/j.ultsonch.2017.12.052>
- [14] K. Deshmukh, M.B. Ahamed, K.K. Sadasivuni, D. Ponnamma, M.A.-A. AlMaadeed, R.R. Deshmukh, S.K. Khadheer Pasha, A.R. Polu, and K. Chidambaram. *J. Appl. Polymer Sci.* **134**, 5, 44427 (2017). <https://doi.org/10.1002/app.44427>
- [15] B.M. Baraker, and B. Lobo. *Can. J. Phys.* **95**, 8, 738 (2017). <https://doi.org/10.1139/cjp2016-0848>
- [16] H.E. Ali, H.S.M. Abd-Rabboh, N.S. Awwad, H. Algarni, M.A. Sayed, A.F.A. El-Rehim, M.M. Abdel-Aziz, and Y. Khairy. *Optik* **247**, 167863 (2021). <https://doi.org/10.1016/j.ijleo.2021.167863>
- [17] S. Choudhary. *J. Mater. Sci.: Mater Electron.* **29**, 12, 10517 (2018). <https://doi.org/10.1007/s10854-018-9116-y>
- [18] A. Kumbhar, L. Spinu, A. Agnoli, K.-Y. Wang, W.L. Zhou, and C.J. O'Connor. *IEEE Trans. Magn.* **37**, 4, 2216 (2001). <https://doi.org/10.1109/20.951128>
- [19] H.A. Hagelin-Weaver, G.B. Hoflund, D.M. Minahan, and G.N. Salaita. *Appl. Surf. Sci.* **235**, 4, 420 (2004). <https://doi.org/10.1016/j.apsusc.2004.02.062>
- [20] N.A.M. Barakat, M.S. Khil, F.A. Sheikh, and H.Y. Kim. *J. Phys. Chem. C* **112**, 32, 12225 (2008). <https://doi.org/10.1021/jp8027353>
- [21] M. Manjunatha, G. Srinivas Reddy, K.J. Mallikarjunaiah, R. Damle, and K.P. Ramesh. *J. Supercond. Nov. Magn.* **32**, 3201 (2019). <https://doi.org/10.1007/s10948-019-5083-7>
- [22] R.M. Ahmed, A.A. Ibrahiem, and E.A. El-Said. *Opt. Spectroscop.* **128**, 5, 642 (2020). <https://doi.org/10.1134/S0030400X20050033>
- [23] E.M. Abdelrazek, I.S. Elashmawi, A. El-Khodary, and A. Yassin. *Curr. Appl. Phys.* **10**, 2, 607 (2010). <https://doi.org/10.1016/j.cap.2009.08.005>
- [24] M.T. Ramesan, P. Jayakrishnan, T. Anilkumar, and G. Mathew. *J. Mater. Sci.: Mater Electron.* **29**, 3, 1992 (2018). <https://doi.org/10.1007/s10854-017-8110-0>
- [25] H. Elhosiny Ali, M.M. Abdel-Aziz, H. Algarni, I.S. Yahia and Y. Khairy. *J. Inorg. Organomet. Polymer Mater.* **31**, 4, 1503 (2021). <https://doi.org/10.1007/s10904-020-01785-2>
- [26] M. Manjunatha, G.S. Reddy, K.J. Mallikarjunaiah, R. Damle and K.P. Ramesh. *J. Supercond. Novel Magn.* **32**, 10, 3201 (2019). <https://doi.org/10.1007/s10948-019-5083-7>
- [27] S. Choudhary, and R.J. Sengwa. *Curr. Appl. Phys.* **18**, 9, 1041 (2018). <https://doi.org/10.1016/j.cap.2018.05.023>
- [28] M. Irfan, A. Manjunath, S.S. Mahesh, R. Somashekar, and T. Demappa. *J. Mater.Sci.: Mater Electron.* **32**, 5, 5520 (2021). <https://doi.org/10.1007/s10854-021-05274-1>
- [29] V. Siva, D. Vanitha, A. Murugan, A. Shameem, and S.A. Bahadur. *Compos. Commun.* **23**, 100597 (2021). <https://doi.org/10.1016/j.coco.2020.100597>

- [30] H.M. Zidan, E.M. Abdelrazek, A.M. Abdelghany, and A.E. Tarabiah. *J. Mater. Res. Technol.* **8**, 1, 904 (2019). <https://doi.org/10.1016/j.jmrt.2018.04.023>
- [31] Q. Wei, Y. Zhang, Y. Wang, W. Chai, and M. Yang. *Mater. Design* **103**, 249 (2016). <https://doi.org/10.1016/j.matdes.2016.04.087>
- [32] E.M. Abdelrazek, I.S. Elashmawi, and S. Labeeb. *Physica B* **405**, 8, 2021 (2010). <https://doi.org/10.1016/j.physb.2010.01.095>
- [33] A. Hashim, and Q. Hadi. *J. Inorg. Organomet. Polymer Mater.* **28**, 4, 1394 (2018). <https://doi.org/10.1007/s10904-018-0837-4>
- [34] S.B. Aziz, M.A. Rasheed, A.M. Hussein, and H.M. Ahmed. *Mater. Sci. Semicond. Proc.* **71**, 197 (2017). <https://doi.org/10.1016/j.mssp.2017.05.035>
- [35] M.E. Sánchez Vergara, A. Ortiz Rebollo, J.R. Alvarez and M. Rivera. *J. Phys. Chem. Solids* **69**, 1, 1 (2008). <https://doi.org/10.1016/j.jpcs.2007.07.084>
- [36] M. Ghanipour, and D. Dorrani. *J. Nanomater.* **2013**, 897043 (2013). <https://doi.org/10.1155/2013/897043>
- [37] M.A. Morsi, A.H. Oraby, A.G. Elshahawy, and R.M. Abd El-Hady. *J. Mater. Res. Technol.* **8**, 6, 5996 (2019). <https://doi.org/10.1016/j.jmrt.2019.09.074>
- [38] H.E. Ali, M.M. Abdel-Aziz, Y. Khairy, H.Y. Zahran, H. Algarni, I.S. Yahia, E.F. El-Shamy, M.A. Sayed, F.A. Maged, and M.F. Sanaa. *Physica Scripta* **96**, 11, 115804 (2021). <http://dx.doi.org/10.1088/1402-4896/ac13e3>
- [39] P.K. Singh, S.K. Tripathi, and D.K. Dwivedi. *Mater. Sci.-Poland* **37**, 4, 554 (2019). <https://doi.org/10.2478/msp-2019-0061>
- [40] A.S. Hassanien, I.M. El Radaf, and A.A. Akl. *J. Alloys. Compd.* **849**, 156718 (2020). <https://doi.org/10.1016/j.jallcom.2020.156718>
- [41] N. Ahlawat, S. Sanghi, A. Agarwal, and S. Rani. *J. Alloys. Compd.* **480**, 2, 516 (2009). <https://doi.org/10.1016/j.jallcom.2009.01.116>
- [42] Y. Khairy, M.M. Abdel-Aziz, H. Algarni, A.M. Alshehri, I.S. Yahia, and H.E. Ali. *Mater. Res. Exp.* **6**, 11, 115346 (2019). <http://dx.doi.org/10.1088/2053-1591/ab4e34>
- [43] A.H. Ammar, A.A.M. Farag, and M.S. Abo-Ghazala. *J. Alloys. Compd.* **694**, 752 (2017). <https://doi.org/10.1016/j.jallcom.2016.10.042>
- [44] C. Li, Q. Xiao, Y. Fu, Y. Liang, C. Liu, Y. Zhuang and L. Xia. *J. Non-Crystal. Solids* **552**, 120453 (2021). <https://doi.org/10.1016/j.jnoncrysol.2020.120453>
- [45] Y. Khairy, I.S. Yahia, and H. Elhosiny Ali. *J. Mater. Sci.:Mater Electron.* **31**, 10, 8072 (2020). <https://doi.org/10.1007/s10854-020-03348-0>
- [46] H.E. Ali, and Y. Khairy. *Vacuum* **180**, 109640 (2020). <https://doi.org/10.1016/j.vacuum.2020.109640>
- [47] H. Elhosiny Ali, H. Algarni, I.S. Yahia, and Y. Khairy. *Chinese J. Phys.* **72**, 270 (2021). <https://doi.org/10.1016/j.cjph.2021.04.022>
- [48] A. Hadi, A. Hashim, and Y. Al-Khafaji. *Trans. Electrical. Electron. Mater.* **21**, 3, 283 (2020). <https://doi.org/10.1007/s42341-020-00189-w>
- [49] A. Lösche. *Krist. Technik.* **7**, 4, K55 (1972). <https://doi.org/10.1002/crat.19720070420>
- [50] F. Yakuphanoglu, and C. Viswanathan. *J. Non-Cryst. Solids* **353**, 30, 2934 (2007). <https://doi.org/10.1016/j.jnoncrysol.2007.06.055>
- [51] R. Pöttsch, B.C. Stahl, H. Komber, C.J. Hawker, and B.I. Voit. *Polym. Chem.* **5**, 8, 2911 (2014). <http://dx.doi.org/10.1039/C3PY01740K>
- [52] H. Elhosiny Ali, I.S. Yahia, H. Algarni, and Y. Khairy. *New J. Phys.* **23**, 4, 043001 (2021). <https://doi.org/10.1088/1367-2630/abe614>
- [53] H. Bao, and X. Ruan. *Int. J. Heat. Mass. Transfer* **53**, 7–8, 1308 (2010). <https://doi.org/10.1016/j.ijheatmasstransfer.2009.12.033>
- [54] O.G. Abdullah, S.B. Aziz, K.M. Omer, and Y.M. Salih. *J. Mater.Sci.: Mater Electron.* **26**, 7, 5303 (2015). <https://doi.org/10.1007/s10854-015-3067-3>
- [55] F.M. Hossain, L. Sheppard, J. Nowotny, and G.E. Murch. *J. Phys. Chem. Solids* **69**, 7, 1820 (2008). <https://doi.org/10.1016/j.jpcs.2008.01.017>
- [56] V. Ganesh, I.S. Yahia, S. AlFaify, and M. Shkir. *J. Phys. Chem. Solids* **100**, 115 (2017). <https://doi.org/10.1016/j.jpcs.2016.09.022>
- [57] H. Elhosiny Ali, M.M. Abdel-Aziz, A.M. Nawar, H. Algarni, H.Y. Zahran, I.S. Yahia, and Y. Khairy. *Polym. Adv. Technol.* **32**, 3, 1011 (2020). <https://doi.org/10.1002/pat.5149>